Brushless dc Motor Control without Position and Speed Sensors

Nobuyuki Matsui, *Member, IEEE,* and Masakane Shigyo

Abstract—**Generally, a brushless dc motor requires a rotor position sensor for commutation and current control. Resolvers and absolute encoders are used as a position sensor, but they increase cost and size of the motor and restrict the industrial drive applications. Furthermore, as the application field expands, the brushless dc motor is used in a special case where the motor cannot be provided with the position sensor. From these backgrounds, position sensor elimination methods have received wide attention.**

This paper presents a new control strategy for a brushless dc motor without position and speed sensors. The control is performed by software using DSP-TMS320C25. The prototype has been constructed using a 1.5-kW, 154-V, 2000-r/min, four-pole motor. The test results have been found satisfactory in both steady and transient states.

Introduction

THEORETICALLY, the brushless dc motor requires a rotor position sensor with which commutation and current control are performed. However, the position sensors such as resolvers and absolute encoders increase cost and size of the motor and restrict its application [1]. Furthermore, as the application fields expand, the brushless dc motor is used in a special case where the motor cannot be provided with a position sensor. From these backgrounds, position sensorless operation of a brushless dc motor has received wide attention.

This paper presents a new control strategy for a brushless dc motor without position and speed sensors. Many papers have reported on the sensorless operation of the brushless motor. The typical and well-known method is the one [2], [3] using induced emf. Since induced emf is proportional to rotor speed, sensorless operation finds difficulties in starting and low-speed range. Another interesting method [4] is reported where the on/off state of the inverter switching devices is used for the rotor position estimation. The method is ingenious but is based on the motor with a trapezoidal emf. Therefore, the method cannot be directly applicable to the motor with a sinusoidal emf.

The control strategy proposed in this paper, on the other hand, is developed on the basis of the instantaneous voltage equation of the brushless dc motor with a sinusoidal flux distribution. Without position sensor, the controller has no information about rotor position, and therefore, the controller determines the applied voltage according to the hypothetical rotor position, which is not necessarily coincident with the actual rotor position. Since the voltage supplied through the inverter is the actual applied voltage, it can be measured. Under the ideal condition that the hypothetical rotor position is coincident with the actual one, the ideal applied voltage can be calculated by using the instantaneous voltage equation of the motor and the detected current. The analysis shows that the difference between the actual and the ideal voltages is proportional to the angular difference between hypothetical and actual rotor positions. Therefore, self-synchronization is possible by reducing the angular difference to zero. Once the rotor position is estimated, the motor speed can be calculated. Thus, the motor can be operated without position and speed sensors. Furthermore, in this control algorithm, the actual applied voltage can be obtained in the controller by calculation (not by measurements) with a knowledge of the PWM pattern, the dead time information, and the dc voltage value. As a result, the control algorithm can be implemented only with the conventional current sensor–no additional sensor is necessary for the proposed sensorless operation.

The complete control system has been constructed using a 1.5-kW, 154-V, 2000-r/min, four-pole motor with sinusoidal flux distribution. The control has been performed by software using a DSP-TMS320C25. The test results have been found satisfactory in steady and transient states.

Sensorless Control Algorithm

Fig. 1 shows the analytical model of the brushless dc motor with a sinusoidal flux distribution. Here, the permanent magnet rotor is represented by the constant dc exciting current and the field winding. In the figure, two rectangular coordinate systems (the $d - q$ and $\gamma - \delta$ axes) are defined. As is apparent from the figure, the direction of the d axis corresponds to the actual rotor flux axis, whereas the $\gamma - \delta$ axis is the hypothetical coordinate system assumed in the controller. Since the $\gamma - \delta$ axis is assumed appropriately, the direction of the γ axis is not necessarily coincident with the rotor axis (the d axis). Therefore these two coordinate systems have an angular difference $\Delta\theta$ as shown below:

$$\Delta\theta = \theta_c - \theta \tag{1}$$

where θ is the actual angle, and θ_c is the hypothetical rotor angle.

Manuscript IPCSD 91-56, approved by the Industrial Drives Committee of the IEEE Industry Applications Society for presentation at the 1990 Industry Applications Society Annual Meeting, Seattle, WA, October 7-12. Manuscript released for publication April 16, 1991.

N. Matsui is with the Department of Electrical and Computer Engineering, Nagoya Institute of Technology, Nagoya, Japan.

M. Shigyo is with Omika Works, Hitachi Ltd., Hitachi, Japan.

IEEE Log Number 9104086.

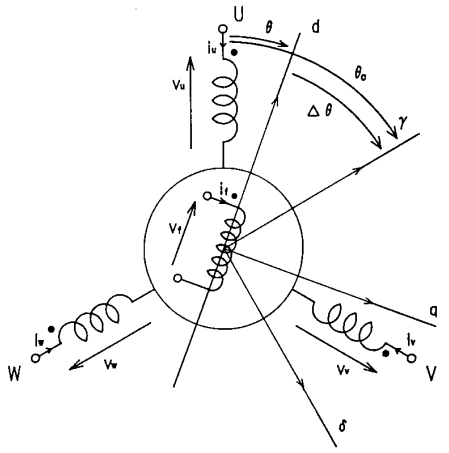

Fig. 1. Analytical model of brushless dc motor.

The voltage equation of the motor is given by the following equation:

$$\begin{bmatrix} v_f \\ v_u \\ v_v \\ v_w \end{bmatrix} = \begin{bmatrix} R_f + PL_f & PM_3 \cos\theta & PM_3 \cos\left(\theta - \frac{2\pi}{3}\right) & PM_3 \cos\left(\theta + \frac{2\pi}{3}\right) \\ PM_3 \cos\theta & R_a + PL_a & PL_a \cos\frac{4\pi}{3} & PL_a \cos\frac{2\pi}{3} \\ PM_3 \cos\left(\theta - \frac{2\pi}{3}\right) & PL_a \cos\frac{4\pi}{3} & R_a + PL_a & PL_a \cos\frac{2\pi}{3} \\ PM_3 \cos\left(\theta + \frac{2\pi}{3}\right) & PL_a \cos\frac{2\pi}{3} & PL_a \cos\frac{4\pi}{3} & R_a + PL_a \end{bmatrix} \begin{bmatrix} i_f \\ i_u \\ i_v \\ i_w \end{bmatrix}. \quad (2)$$

The three-phase components can be transformed into the $\gamma - \delta$ axis components using the well-known transformation matrix given below:

$$\begin{bmatrix} \gamma \\ \delta \end{bmatrix} = \sqrt{\frac{2}{3}} \cdot \begin{bmatrix} \cos\theta_c & \cos\left(\theta_c - \frac{2\pi}{3}\right) & \cos\left(\theta_c + \frac{2\pi}{3}\right) \\ -\sin\theta_c & -\sin\left(\theta_c - \frac{2\pi}{3}\right) & -\sin\left(\theta_c + \frac{2\pi}{3}\right) \end{bmatrix} \cdot \begin{bmatrix} U \\ V \\ W \end{bmatrix}. \quad (3)$$

The $\gamma - \delta$ axis voltage equation can be obtained by combining (1)–(3) under the assumption that the exciting current i_f is constant and is equal to I_f:

$$\begin{bmatrix} v_\gamma \\ v_\delta \end{bmatrix} = \begin{bmatrix} R + LP & -L\dot{\theta}_c \\ L\dot{\theta}_c & R + LP \end{bmatrix} \begin{bmatrix} i_\gamma \\ i_\delta \end{bmatrix} + K_E\dot{\theta} \begin{bmatrix} \sin\Delta\theta \\ \cos\Delta\theta \end{bmatrix} \quad (4)$$

where v_γ and v_δ are the actual applied voltages, and i_γ and i_δ are the actual currents, all transformed to the $\gamma - \delta$ axis. R and L are the armature resistance and inductance, and K_E is the emf constant on the basis of the $\gamma - \delta$ axis and are related to the three phase parameters as follows:

$$R = R_a, \quad L = \frac{3}{2}L_a, \quad M = \sqrt{\frac{3}{2}}M_3, \quad K_E = MI_f. \quad (5)$$

The hypothetical and actual rotor speeds are represented as

$$\dot{\theta}_c = \frac{d\theta_c}{dt}, \quad \dot{\theta} = \frac{d\theta}{dt}. \quad (6)$$

Assuming the ideal operating condition that $\Delta\theta = 0$ and $\dot{\theta}_c = \dot{\theta}$, the voltage equation, based on the $d - q$ axis in Fig. 1, can be obtained as follows:

$$\begin{bmatrix} v'_\gamma \\ v'_\delta \end{bmatrix} = \begin{bmatrix} R + LP & -L\dot{\theta}_c \\ L\dot{\theta}_c & R + LP \end{bmatrix} \begin{bmatrix} i_\gamma \\ i_\delta \end{bmatrix} + K_E\dot{\theta}_c \begin{bmatrix} 0 \\ 1 \end{bmatrix}. \quad (7)$$

Since v_γ' and v_δ' in (7) are hypothetical voltages, they cannot be detected. However, these hypothetical voltages can be calculated using the actual line current transformed to the $\gamma - \delta$ axis.

Using the γ axis components in (4) and (7), the γ axis voltage difference Δv_γ can be given by the following relation:

$$\Delta v_\gamma = v_\gamma - v'_\gamma = K_E\dot{\theta}\sin\Delta\theta. \quad (8)$$

Under the condition that $\dot{\theta} \neq 0$ and $\Delta\theta \simeq 0$, (8) is approximated as follows:

$$\Delta v_\gamma = v_\gamma - v'_\gamma \propto \Delta\theta. \quad (9)$$

This equation indicates that the angular difference between the actual and hypothetical axes can be estimated by the voltage difference between the actual and hypothetical axes. As stated, the voltage difference can be obtained in the controller because the actual voltage can be detected, and the hypothetical voltage can be calculated using the detected current.

It is noted here that the actual applied voltage can also be obtained by calculation (not by detection) using the dc voltage, PWM pattern, and the dead time information. Therefore, estimation of angular difference can be calculated in the controller, that is, no additional sensor is needed to estimate the angular difference. Only the current detection, which is very common in the conventional controller, is necessary.

Self Synchronization

As stated above, the angular difference between the hypothetical and actual coordinate systems is proportional to the voltage difference. Once the angular difference $\Delta\theta$ in Fig. 1 is estimated, self synchronization can be achieved by increasing the rotational speed $\dot{\theta}_c$ of the hypothetical axis for $\Delta\theta < 0$ and decreasing it for $\Delta\theta > 0$. This processing is well explained in Fig. 2. According to Fig. 2, the self-synchronization mechanism will be given in the following.

First, the rotor speed $\dot{\theta}$ should be estimated because the system has no speed sensor. Using the δ axis component in (4), the rotor speed can be estimated by the following relation under the assumption that $\Delta\theta \simeq 0$ and $\dot{\theta}_c \simeq \dot{\theta}$:

$$\hat{\dot{\theta}} = \frac{v_\delta - (R + LP)i_\delta}{K_E + Li_\gamma}. \tag{10}$$

Since position is given as an integral of speed, the angular difference $\Delta\theta$ would reach zero by adjusting the correction speed α defined by (11):

$$\alpha = \dot{\theta}_c - \hat{\dot{\theta}}. \tag{11}$$

Here, the actual rotor speed $\dot{\theta}$ is replaced with the estimated rotor speed $\hat{\dot{\theta}}$.

For clockwise rotation in Fig. 1, the following conclusion would result to make $\Delta\theta = 0$ by combining (9) and (11):

$$\begin{cases} \text{if} \quad \Delta\theta > 0 (\Delta v_\gamma > 0), & \text{then } \alpha < 0 \\ \text{if} \quad \Delta\theta < 0 (\Delta v_\gamma < 0), & \text{then } \alpha > 0. \end{cases} \tag{12}$$

For counterclockwise rotation, (12) should be changed as follows:

$$\begin{cases} \text{if} \quad \Delta\theta > 0 (\Delta v_\gamma > 0), & \text{then } \alpha > 0 \\ \text{if} \quad \Delta\theta < 0 (\Delta v_\gamma < 0), & \text{then } \alpha < 0. \end{cases} \tag{13}$$

Although (12) and (13) can be implemented in many ways, the *PI* algorithm is used here:

$$\alpha = \left(K_{SP}\Delta v_\gamma + K_{SI} \int \Delta v_\gamma \, dt \right) \operatorname{sgn}(\dot{\theta}_c). \tag{14}$$

Basic Control Concept

According to the proposed control algorithm, the basic control system configuration is summed up as shown in Fig. 3. Referring to Fig. 3, the following control processing is performed:

1) Three-phase current is detected. Three-phase voltage is obtained not by detection but by calculation in the controller using the dc voltage, PWM pattern, and dead time information.
2) Three-phase voltage and current are transformed to the $\gamma - \delta$ axis voltage and current.
3) The estimated rotor speed is calculated according to (10).
4) The actual voltage is already known from step 1. The hypothetical voltage given in (7) is calculated using the detected current.
5) The angular difference $\Delta\theta$ can be determined by using (9).
6) The correction speed α is determined according to (14).
7) $\dot{\theta}_c$ is modified according to (11).
8) $\dot{\theta}_c$ is compared with the speed command $\dot{\theta}^*$. The speed error $\Delta\dot{\theta} = \dot{\theta}^* - \dot{\theta}_c$ is the input of the *PI* speed regulator, and the torque current command i_δ^* is obtained as the output of the speed regulator.
9) The current commands are compared with the transformed currents, and the PWM pattern is selected to regulate the motor current.

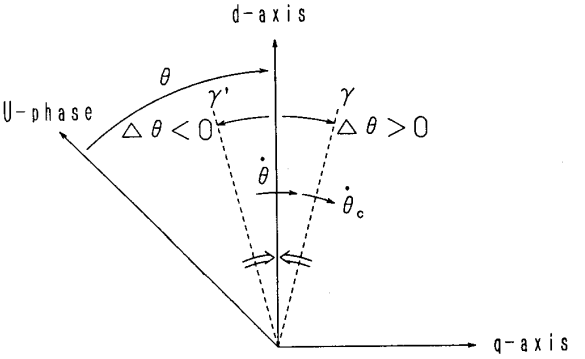

Fig. 2. Self-synchronization mechanism.

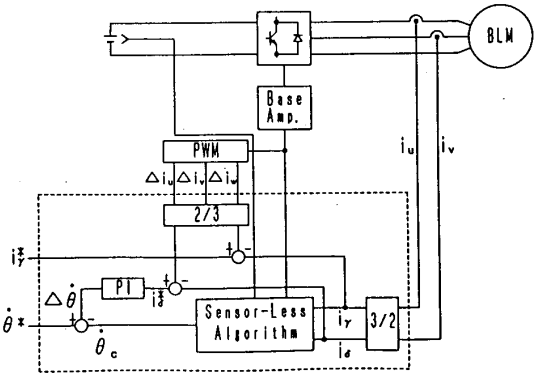

Fig. 3. System configuration.

Simulation Results

The adequacy of the proposed control algorithm was verified by simulation. In the simulation, some assumptions were made as follows:

1) The initial conditions are $\Delta\theta = \Delta, \dot{\theta} = \dot{\theta}_c = 0$; voltages and currents are zero.
2) The applied voltage and the line current are detected exactly without time delay.
3) Exact arithmetic operations are performed in the controller.
4) In the simulation of the inverter, the dead time and turn on/off time of transistors are taken into account.
5) Current control is performed with a software-implemented current hysteresis-controlled PWM.

6) The motor is treated as follows: Rearranging (2)

$$\frac{d}{dt}i_u = \frac{2}{3L_a}(v_u - R_a i_u + K_{E3}\cdot\dot{\theta}\sin\theta)$$

$$\frac{d}{dt}i_v = \frac{2}{3L_a}\left\{v_v - R_a i_v + K_{E3}\cdot\dot{\theta}\sin\left(\theta - \frac{2}{3}\pi\right)\right\} \tag{15}$$

$$\frac{d\theta}{dt} = \dot{\theta}$$

where K_{E3} is the emf constant for the three-phase model. The mechanical equation of the motor is given as follows:

$$\frac{d}{dt}\dot{\theta} = \frac{\lambda}{J}(\tau - T_L - D\omega_m)$$

$$\omega_m = \frac{\dot{\theta}}{\lambda} \tag{16}$$

where

- λ number of pole pair
- τ generated torque of motor
- T_L load torque
- D frictional constant
- ω_m rotor speed.

The generated torque can be given below:

$$\tau = \lambda K_{E3}\left\{i_u\sin\theta + i_v\sin\left(\theta - \frac{2}{3}\pi\right) - (i_u + i_v)\sin\left(\theta + \frac{2}{3}\pi\right)\right\}. \tag{17}$$

Using (15)-(17), the current for each current control period can be obtained for a given PWM pattern when the control procedure previously explained in the Basic Control Concept section of this paper is followed.

Motor specifications (two-phase model) and system constants are shown in Tables I and II, respectively. Current detection is an important factor for the sensorless operation because the control algorithm is based on the instantaneous voltage equation. As stated, current control is performed by the software-implemented current hysteresis-controlled PWM, and the resulting current waveform in a current control period T_c is shown in Fig. 4. In Fig. 4, current is detected at sampling point $n-1$ and is compared with the reference to determine the new PWM pattern $PAT(n-1)$. This processing requires T_d, and therefore, the PWM pattern is changed, if necessary, after T_d from the sampling point and the same pattern continues during the current control period. Referring to Fig. 4, it is concluded that the current detection should be performed in the following manner:

1) Current should be sampled during the latter half period to avoid noises included in current due to commutation.
2) Current should be sampled after the PWM pattern is changed to avoid the effects of transient caused by the turn on/off of transistors.

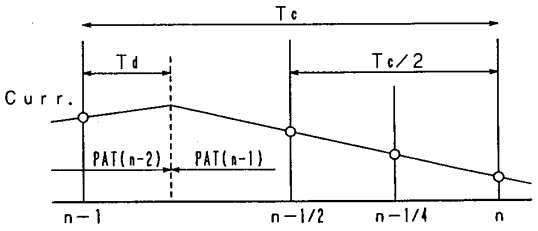

Fig. 4. Sampling timings for current detections: T_c—current control period; T_d—delay time due to control processing and dead time of inverter: $PAT(x)$—PWM pattern between sampling point x and $x+1$.

TABLE I
MOTOR SPECIFICATIONS

no. of pole pair	2
rated output	1.5 kW
rate current	7.5 A
rated voltage	154 V
rated speed	2000 r/min
rated torque	73 kg-cm
rotor inertia	0.048 kg-m^2
frictional const.	0.0042 kg-m^2/s
armature resist.	0.95 Ω
armature induct.	5.11 mH
torque const.	0.28 Nm/A

TABLE II
SYSTEM CONSTANTS

curr. cont'l period	200 μs
speed cont'l period	1.6 ms
dead time	24 μs
t_{on}/t_{off}	3/16 μs
K_{SP}/K_{SI} (gains of (14))	0.06/0.001
K_{CP}/K_{CI} (gains of speed regulator)	1.02/0.004

Taking these items into account, (8) and (10) are modified as discrete equations:

$$\Delta v_\gamma\left(n-\frac{1}{4}\right) = v_\gamma\left(n-\frac{1}{4}\right) - v'_\gamma\left(n-\frac{1}{4}\right)$$
$$= -Ri_\gamma\left(n-\frac{1}{4}\right) - \frac{L}{T}\left\{i_\gamma(n) - i_\gamma\left(n-\frac{1}{2}\right)\right\}$$
$$+ \dot{\theta}_c(n-1)Li_\delta\left(n-\frac{1}{4}\right) + v_\gamma\left(n-\frac{1}{4}\right) \tag{18}$$

$$\dot{\theta}\left(n-\frac{1}{4}\right) = \frac{v_\delta\left(n-\frac{1}{4}\right) - Ri_\delta\left(n-\frac{1}{4}\right) - \frac{L}{T}\left\{i_\gamma(n) - i_\delta\left(n-\frac{1}{2}\right)\right\}}{K_E + Li_\gamma\left(n-\frac{1}{4}\right)}. \tag{19}$$

Fig. 5 shows the simulation results for starting under initial conditions $\theta = \theta_c = 0$ ($\Delta\theta = 0$). As shown in the figure, the hypothetical speed has an error immediately after starting, and therefore, $\Delta\theta$ increases temporarily after starting. However, these phenomena are temporary, and $\Delta\theta$ converges to zero.

Fig. 6 is the extreme case where $\theta = 0, \Delta\theta = 65°$. Even

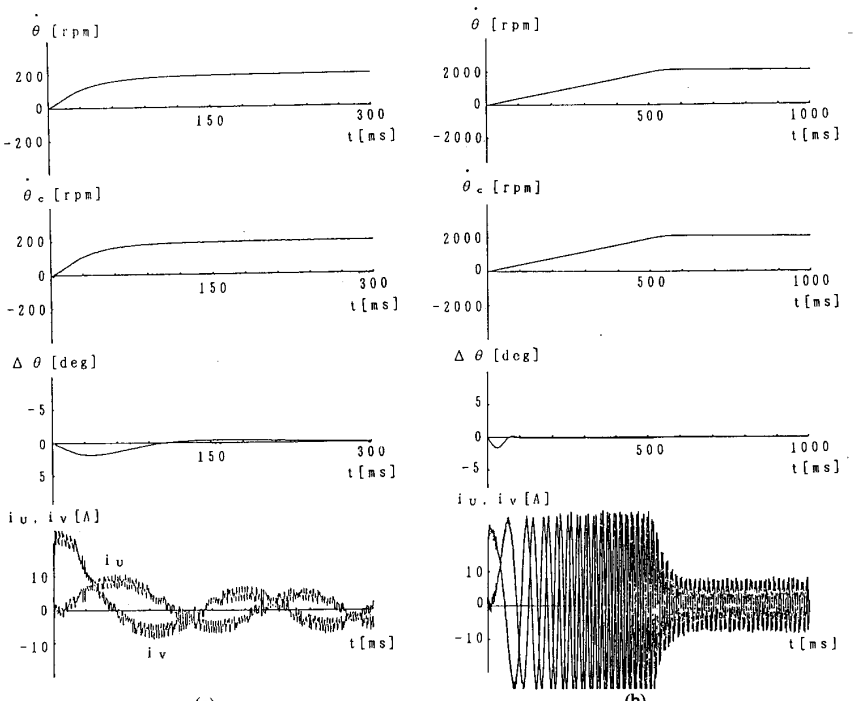

Fig. 5. Simulation results for starting under initial condition $\theta = \theta_c = 0$: (a) Final speed 200 r/min; (b) final speed 2000 r/min.

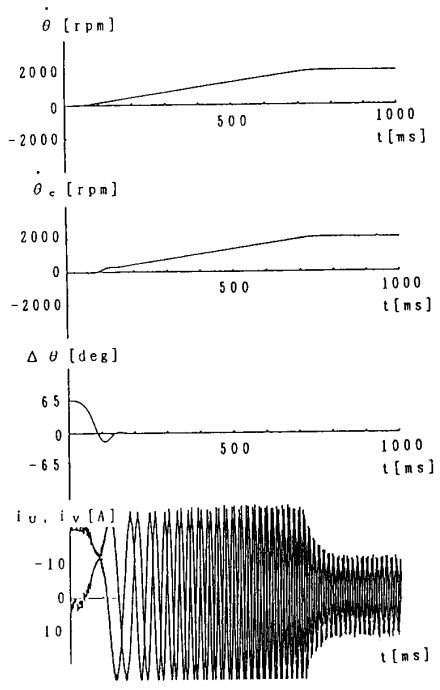

Fig. 6. Simulation results for starting under initial conditions $\theta = 0$, $\Delta\theta = 65°$.

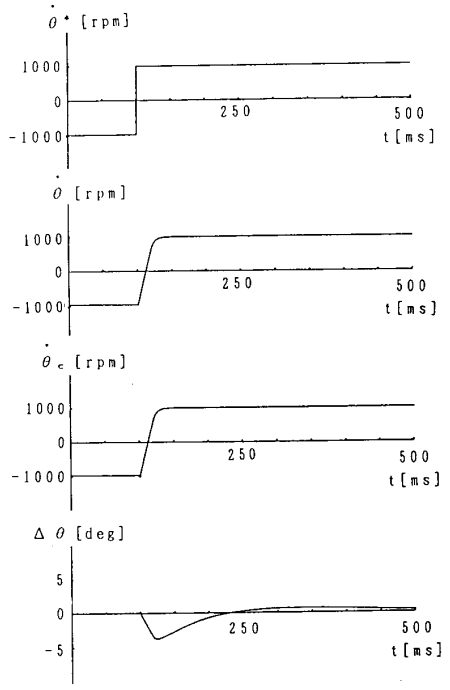

Fig. 7. Simulation results for four-quadrant operation.

in such an extreme case, the stable starting can be obtained. However, the stable starting could not be obtained for $\Delta\theta > 65°$. A certain auxiliary starting is necessary in practice, which will be explained later.

Fig. 7 is the four-quadrant operation for the stepwise reference speed from -1000 to $+1000$ r/min. Similar to the starting characteristics, $\Delta\theta$ increases temporarily, immediately after the reference change, but after that, it converges to zero. The maximum error is within 5°.

Fig. 8 shows the effect of parameter changes on the

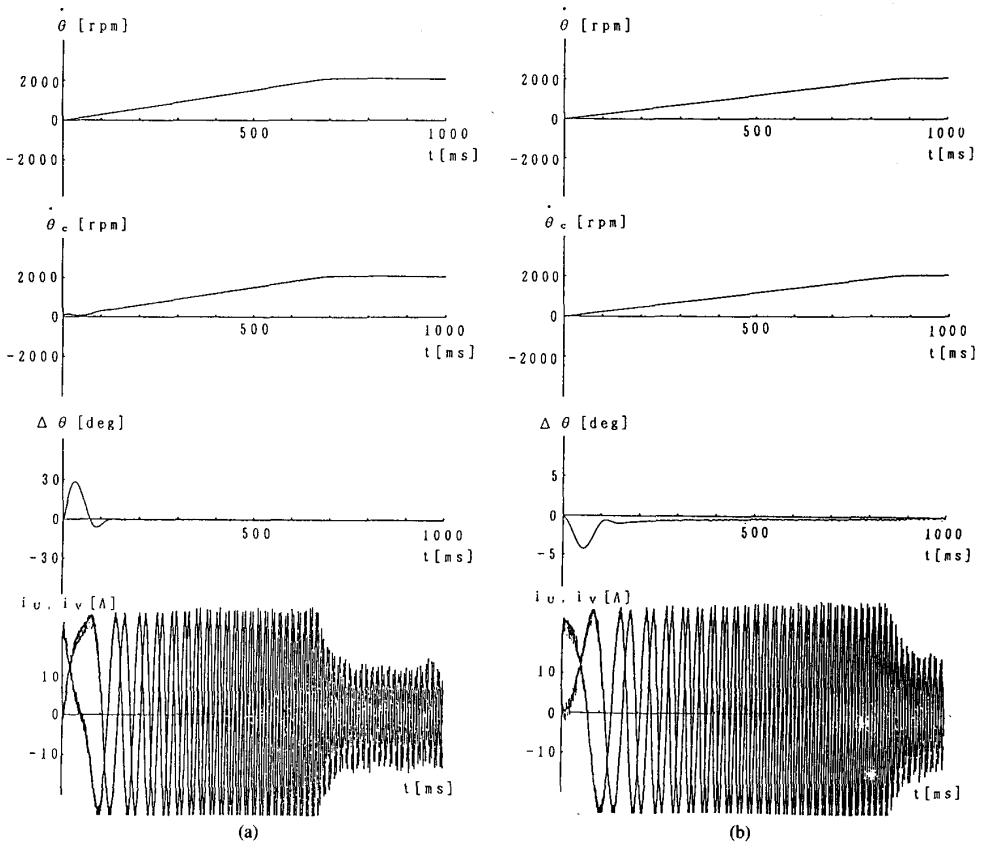

Fig. 8. Effects of parameter changes on starting characteristics: (a) Resistance increased by 30%; (b) emf constants reduced by 15%.

starting characteristics. Assuming the temperature rise of 80°C, the winding resistance increases by 30%, and flux decreases by 15% in the case of a ferrite magnet [5]. Inductance is not affected by temperature. Fig. 8(a) shows the case when winding resistance is increased by 30%, and (b) corresponds to the case when the emf constant is decreased by 15%, respectively. The angular difference immediately after starting becomes larger, and convergence is a little slower, but stable starting is possible.

It is noted here that robust sensorless operation is possible by combining the proposed algorithm with a real-time parameter identification [5].

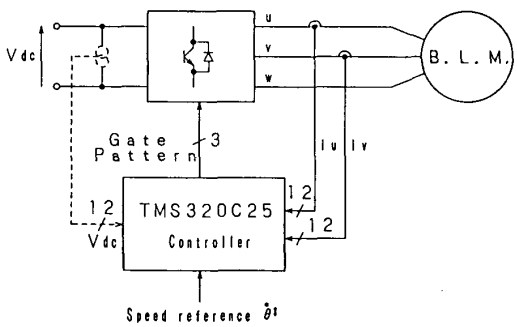

Fig. 9. Experimental system configuration.

Experimental Results

Fig. 9 shows an experimental system. The motor specifications are given in Table I, and the following experimental data were obtained under the no-load condition. The transistor inverter was used, and the dc voltage was 280 V. The 12-b A/D converter was used for current detection, and the resolution was 0.022A/b. As stated, the phase voltage, which is necessary to perform the control algorithm, was obtained by calculations (not by a sensor) using the dc voltage, PWM pattern, and dead time information to eliminate the noise-sensitive ac voltage detector. The dc voltage detection shown with the dotted line in the figure is necessary only when the dc voltage is varied. A DSP-TMS320C25 was used in the controller, and the current control period was 200 μs, whereas the speed control period was 1.6 ms.

The starting procedure of the motor is as follows. A specified PWM pattern (e.g., a U-phase upper transistor, V- and W-phase lower transistors are on) is applied for 200 μs. This is repeated several times; then, the rotor is aligned in the direction of the U-phase winding. Since stable starting is possible for $\Delta\theta < 65°$, as the simulation shows, the motor can be successfully started after the above procedure.

Fig. 10 shows the comparison between actual and esti-

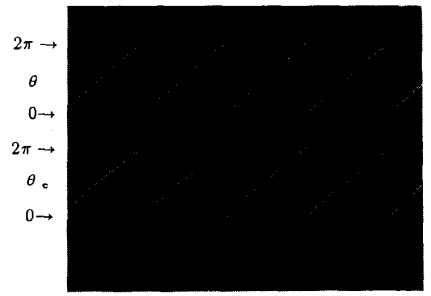

Fig. 10. Actual and estimated positions.

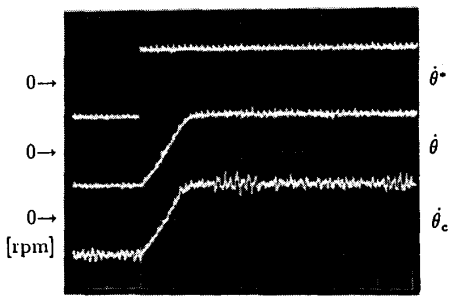

Fig. 12. Reversing characteristics.

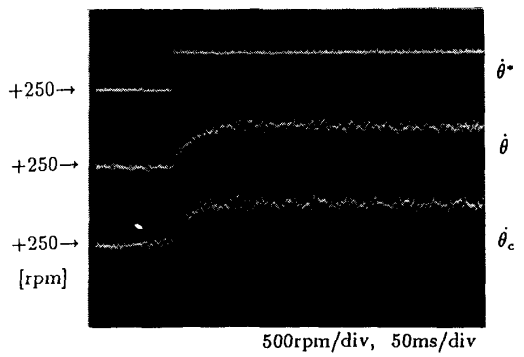

Fig. 11. Step response of speed.

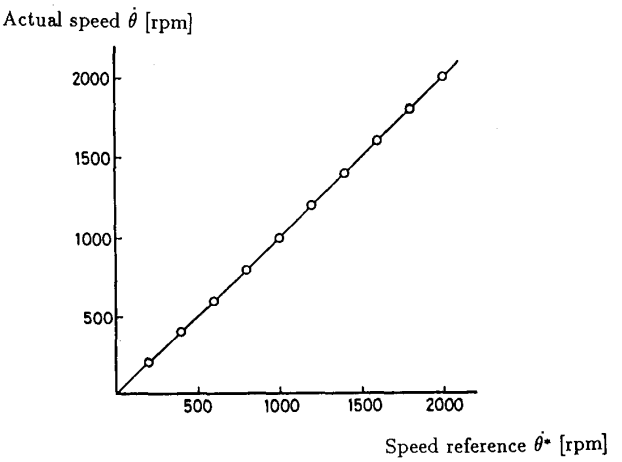

Fig. 13. Speed characteristics versus speed reference.

mated positions under sensorless operation at 250 r/min. The actual position information was obtained from the resolver for measurement. It is observed that close agreement between actual and estimated positions was obtained.

Fig. 11 is a step response of speed when the speed reference changes from 250 to 750 r/min, and Fig. 12 is a reversing characteristic when the speed reference changes from -2000 to $+2000$ r/min where $\dot{\theta}^*$, $\dot{\theta}$, and $\dot{\theta}_c$ are the speed reference, the actual speed, and the estimated speed, respectively. In both cases, the estimated speed shows good agreement with the actual speed, even in transient state. The noise on the experimental tracings originates partly from the D/A converter but largely from the ripple component of the line current. Since $\dot{\theta}_c$ is obtained from (10), the ripple of the detected current directly has an effect on the accuracy of $\dot{\theta}_c$.

Fig. 13 shows the relation between actual and reference speeds.

The following are characteristics under the loaded condition. The steady-state torque-speed characteristics are shown in Fig. 14, where the speed is maintained constant with an accuracy of $\pm 1\%$, independent of load.

Fig. 15 shows $\Delta\theta$ characteristics for a stepwise load torque change. Here, the rated torque is applied and then removed when the speed reference is 400 r/min. An angular difference $\Delta\theta$ increases temporarily immediately after a load change, but it converges to a steady-state level without delay. The steady-state angular difference is approximately within $\pm 5°$.

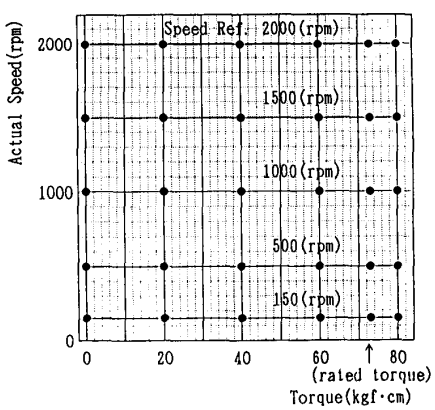

Fig. 14. Steady-state torque-speed characteristics under load.

Conclusions

In this paper, a new control algorithm of a brushless dc motor without position and speed sensors has been proposed and tested. Starting from the instantaneous voltage equation for a brushless dc motor whose rotor position is different from its actual position, conditions have been introduced to reduce the position error to be zero. The adequacy of the

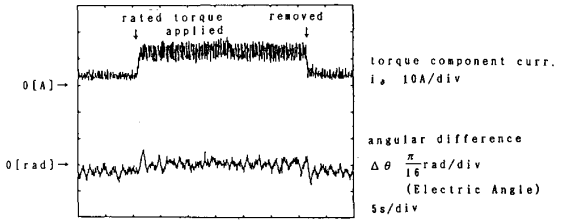

Fig. 15. Characteristics for load change

proposed algorithm has been verified by simulation and experiments.

References

[1] V. R. Stefanovic, "Recent trends in variable ac drives," in *IPEC-Tokyo Conf. Rec.*, 1983, pp. 438–449.

[2] K. Iizuka, H. Uzuhashi, M. Kano, T. Endo, and K. Mohri, "Microcomputer control for sensorless brushless motor," *IEEE Trans. Industry Applications*, vol. IA-21, pp. 595–601, May/June 1985.

[3] M. D. Erdman, H. B. Harms, and J. L. Oldenkamp, "Electronically commutated dc motors for the appliance industry," in *IEEE-IAS Conf. Rec.*, 1984, pp. 1339–1345.

[4] S. Ogasawara and H. Akagi, "An approach to position sensorless drive for brushless dc motors," in *IEEE-IAS Conf. Rec.*, 1990, pp. 443–447.

[5] N. Matsui and H. Ohasi, "DSP-based adaptive control of a brushless motor," in *Proc. IEEE/IAS Ann. Mtg.* (Pittsburgh), 1988.

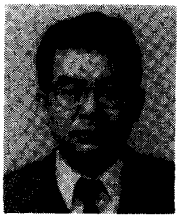

Nobuyuki Matsui (M'90) was born in Wakayama, Japan, on May 7, 1943. He received the B.S. and M.S. degrees in electrical engineering from Nagoya Institute of Technology, Nagoya, Japan, in 1966 and 1968, respectively, and the Ph.D. degree from Tokyo Institute of Technology, Tokyo, Japan, in 1976.

Since 1968, he has been with the Department of Electrical and Computer Engineering, Nagoya Institute of Technology, where he is currently a Professor and is engaged in research on computer control of electric motors.

Dr. Matsui is a member of the Institute of Electrical Engineers of Japan and the Society of Instrument and Control Engineers.

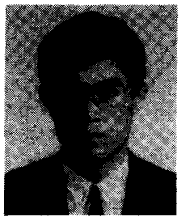

Masakane Shigyo was born in Osaka, Japan, on August 28, 1964. He received the B.S. and M. S. degrees from Nagoya Institute of Technology, Nagoya, Japan in 1988 and 1990, respectively.

In 1990, he joined Omika works, Hitachi Ltd., and is engaged in research and development of power systems.

Mr. Shigyo is a member of the Institute of Electrical Engineers of Japan.